Applied Physics Letters

Melts of CrCoNi-based high-entropy alloys: Atomic diffusion and electronic/atomic structure from *ab initio* simulation

Cite as: Appl. Phys. Lett. **113**, 111902 (2018); https://doi.org/10.1063/1.5045216
Submitted: 18 June 2018 . Accepted: 02 September 2018 . Published Online: 14 September 2018

Jun Ding, Mark Asta, and Robert O. Ritchie

AIP Publishing

Melts of CrCoNi-based high-entropy alloys: Atomic diffusion and electronic/atomic structure from *ab initio* simulation

Jun Ding,[1] Mark Asta,[1,2,a)] and Robert O. Ritchie[1,2,a)]
[1]*Materials Sciences Division, Lawrence Berkeley National Laboratory, Berkeley, California 94720, USA*
[2]*Department of Materials Science and Engineering, University of California, Berkeley, California 94720, USA*

(Received 18 June 2018; accepted 2 September 2018; published online 14 September 2018)

High-entropy alloys (HEAs) are an emerging class of advanced structural alloys under extensive research; yet, the properties of the liquid states of these materials, which are relevant to their processing, have been far less explored. In this work, we utilize *ab initio* molecular dynamics simulations to investigate the melt properties of a representative HEA—the Cantor alloy—and its derivatives: CrMnFeCoNi, CrFeCoNi, and CrCoNi. The atomic dynamics of these melts at various temperatures are investigated, specifically to analyze their electronic and atomic structures, including charge transfer, pair distribution functions, and short-range order. Results are compared with existing information for the liquids of metallic glasses, which also typically contain multiple principal elements, but retain the amorphous state under moderate to fast cooling rates. The present results provide insights into the structural and bonding factors favoring solidification to single-phase solid solutions in HEAs. *Published by AIP Publishing*. https://doi.org/10.1063/1.5045216

High-entropy alloys (HEAs) are an exciting new class of metallic alloys with multiple elements in nominally equal molar ratios that can crystallize as a single phase, despite containing elements with different crystal structures including *fcc*, *hcp*, and *bcc*.[1–5] The stability of these materials was initially understood to result from the configurational entropy contribution to the total free energy, which acts to stabilize the solid-solution state relative to multi-phase microstructures.[1–3] More recently, the importance of enthalpic terms in stabilizing HEAs has been emphasized.[4] HEAs have been intensively investigated and certain of these systems have been found to exhibit exceptional mechanical properties, such as high fracture toughness and high strength, as well as outstanding irradiation-tolerance behavior.[6–10] A prime example is the five-element CrMnFeCoNi alloy (so-called Cantor HEA), which forms a single-phase *fcc* solid solution, and displays exceptional damage tolerance properties that are even further improved at cryogenic temperatures, contrary to behavior in most metallic materials.[6] Another multiple-principal-element alloy with three components, CrCoNi (referred to as a medium-entropy alloy), was found to show even better mechanical properties, with a toughness of 275 MPa $m^{1/2}$ at cryogenic temperatures; its damage-tolerant properties approach the best on record.[7]

The two solid-solution alloys, CrMnFeCoNi and CrCoNi alloys, have been studied extensively by both experiment and simulation.[6,7,11–18] However, the properties of the liquid states of these materials have not been investigated in details. Liquid-phase properties, including, in particular, transport and thermodynamic properties, are of primary importance for understanding and predictive modeling of microstructure evolution in solidification processing of HEAs.[19] These properties, as well as detailed information about the liquid local atomic structure, also provide critically important benchmark results for the development of classical force field models that form the basis for atomic-scale modeling of deformation in these materials. Further, a detailed study of HEA liquid states provides an opportunity to compare with known properties of the melts of another class of emerging structural alloys, metallic glasses (MGs), which are also typically formed from multiple metallic components, but retain the amorphous phase after moderate to fast cooling rates. Despite the importance of liquid-state properties, their experimental measurement in high-temperature melts is challenging, and *ab initio* molecular-dynamics (AIMD) simulations have emerged as a powerful framework for their calculation.

In this work, we employ AIMD simulations to investigate the melts of three representative HEAs with related chemistries: CrMnFeCoNi, CrFeCoNi, and CrCoNi alloys. These compositions can be regarded as CrCoNi-base alloys, with the addition of Fe and Mn elements to form four and five-component HEAs. The atomic dynamics of these melts at various temperatures were studied from analyses of both mean square displacements (MSD) and velocity autocorrelation functions (VACF). Further, we analyze the electronic and atomic structure of the melts, including charge transfer, pair distribution functions (PDFs), and icosahedral short-range order. The results are of particular interest as a basis for comparison with existing information on the liquids of metallic glass systems.[20,21]

The melts of CrMnFeCoNi, CrFeCoNi, and CrCoNi were investigated by AIMD simulations based on density functional theory (DFT), using the Vienna *ab initio* simulation package (VASP).[22,23] The simulated configurations contained 180 atoms in a cubic box with periodic boundary conditions. Projector-augmented-wave (PAW) potentials were employed with the Perdew-Burke-Ernzerhof (PBE) form of the generalized-gradient approximation (GGA) for the exchange-correlation functional.[24–26] The wave-functions were sampled using a single k-point (Γ)[27] and all calculations were performed spin polarized to account for the presence of local magnetic moments.

The simulation systems were initialized as solid solutions with *fcc* crystal structures, with each lattice site occupied

a)Electronic addresses: mdasta@berkeley.edu and roritchie@lbl.gov

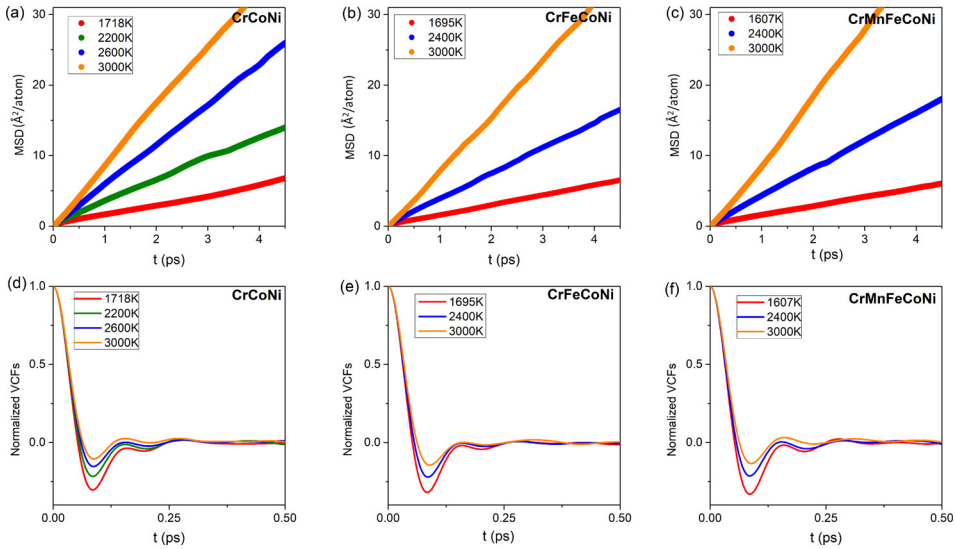

FIG. 1. (a)–(c) Mean square displacement (MSD) and (d)–(f) velocity auto-correlation functions (VACF) as a function of time t, respectively, for the melts of the CrCoNi, CrFeCoNi, and CrMnFeCoNi alloys at different temperatures.

randomly by the different elemental constituents. Subsequently, these samples were melted and equilibrated at high temperature (3000 K) using the constant-temperature, constant-volume (NVT) ensemble for about 10 ps with the time step of 1 fs. The melts were gradually quenched to T_m (liquidus temperature) and another 10 ps relaxation was applied at each studied temperature, followed by adjusting the density to minimize pressure. The values of T_m used in the simulations for the CrMnFeCoNi, CrFeCoNi, and CrCoNi alloys are the experimental estimates of 1607 K, 1695 K, and 1718 K, respectively.[28,29] The electronic structure and short-range order in the melts at T_m were further studied using the inherent structures, which were obtained by relaxing the atoms using the conjugate gradient method. For the melt of each of the three HEAs considered, analyses of charge transfer were conducted on the inherent structures of five independent configurations, using self-consistent charge densities derived from calculations using a k-point mesh of $3 \times 3 \times 3$ for improved accuracy.

The atomic dynamics of the three melts were investigated through calculations of MSD and VACF at various temperatures between 3000 K and the corresponding T_m for the given alloy composition. From these quantities, it is possible to derive the self-diffusion coefficients for each species at each temperature considered. The MSD at time t, $M(t)$, can be defined as[30]

$$M(t) \equiv \frac{1}{N}\sum_{i=1}^{N}\langle (x_i(t) - x_i(0))^2 \rangle, \tag{1}$$

where N is the number of atoms of the melts, and $x_i(t)$ is the position of the ith atom at time t. Figures 1(a)–1(c) shows the calculated MSD of the melts of CrCoNi, CrFeCoNi, and CrMnFeCoNi, respectively, at various temperatures. A linear relationship between M(t) and t can be observed, except at early times where the dynamics are not diffusive.

The velocity auto-correlation function (VACF) is defined as[30]

$$C(t) = \langle v_i(t) \cdot v_i(t=0) \rangle, \tag{2}$$

where $v_i(t)$ are the velocity of atom i at time t, and the angular brackets denote the average over time origins as well as all atoms. Figures 1(d)–1(f) show the computed VACFs [normalized by $\langle v_i(t=0) \cdot v_i(t=0) \rangle$)] at various temperatures. The obvious minima in the VACF indicate the back-scattering regime, where the backflow induced by a moving atom increases the probability of an atom to jump back toward its initial position. The lower the temperature, the deeper the first minimum in their VACF, which reveals the increasing back-scattering effects.[30]

Both the MSD and VACF can lead to the calculation of the self-diffusion coefficient, D, of liquids. Specifically, D values can be derived from the linear slope of the MSD, $M(t)$, as[30]

$$D = \frac{1}{6}\frac{\partial M(t)}{\partial t} = \frac{1}{6}\partial\left(\frac{1}{N}\sum_{i=1}^{N}\langle (x_i(t) - x_i(0))^2 \rangle\right)/\partial t. \tag{3}$$

In addition, the time integration of the VACF also gives access to D, as[30]

$$D = \frac{1}{3}\int_0^\infty C(t)dt. \tag{4}$$

Equations (3) and (4) apply to the self-diffusion coefficient (D_i) for each species type (i). Table I lists the self-diffusion coefficient D_i for each species in the melts of the CrCoNi, CrFeCoNi, and CrMnFeCoNi alloys computed at T_m. In our analyses, we have found that the D_i values for the Cr, Fe, Co, Ni, and Mn species differ by no more than 10%, which is within the statistical precision of the values that can be derived from the present AIMD data. Hence, in Fig. 1 and in what follows we focus on results for the concentration-weighted average of the self-diffusion coefficients: $D = \sum_i D_i \cdot x_i$, where x_i denotes the mole fraction of species i.

Figure 2 summarizes the concentration-weighted average of the self-diffusion coefficients, D, for the CrCoNi-based alloy melts at various temperatures, derived from both the MSD and VACF. As expected, the computed values for D, obtained independently from the MSD and VACF, show excellent agreement. Figure 2 presents an Arrhenius plot of the scaling between D and reciprocal temperature ($1/T$) within the temperature range from T_m to 3000 K. The

TABLE I. The self-diffusion coefficient D_i for each species in the melts of the CrCoNi, CrFeCoNi, and CrMnFeCoNi alloys computed at T_m. Values of D_i for each species are calculated from the MSD [Eq. (3)].

	D_{Cr} (Å^2/ps)	D_{Co} (Å^2/ps)	D_{Ni} (Å^2/ps)	D_{Fe} (Å^2/ps)	D_{Mn} (Å^2/ps)
CrCoNi (1718 K)	0.248	0.243	0.239	…	…
CrFeCoNi (1695 K)	0.241	0.231	0.228	0.223	…
CrMnFeCoNi (1607 K)	0.196	0.182	0.181	0.183	0.193

diffusion activation energy ΔE, defined through a fit to the Arrhenius relationship,[30] $D = D_0 \exp\left(-\frac{\Delta E}{kT}\right)$ (where k is the Boltzmann constant), was calculated to have values for the CrMnFeCoNi, CrFeCoNi and CrCoNi alloys of $\Delta E = 1.70$, 1.71, and 1.64 eV, respectively. The similar values of these activation energies imply that the liquid diffusion dynamics are not strongly affected by the addition of Fe and Mn to the CrCoNi liquid. We note that we are unaware of experimental measurements to which the calculated diffusivities can be compared; however, such comparisons in related transition-metal alloys have shown good agreement between experiments and AIMD results (e.g., Ref. 31).

Figure 3 shows the results of the Bader analysis for charge transfer in the CrMnFeCoNi, CrFeCoNi, and CrCoNi liquids. The Bader analysis was performed by locating the zero flux surfaces, where the gradient of charge density is given by $\nabla\rho(\vec{r}) = 0$, leading to a definition of a volume enclosing each atom; the charge enclosed within this Bader volume can be considered as the total electronic charge of that atom in the structure.[32,33] The difference between the Bader charge so derived, and the original number of valence electrons for the neutral atom, is an indicator of the charge transfer. The positive and negative values for the charge transfers plotted in Figs. 3(a)–3(c) correspond to the average number of electrons received and lost by the given atom, respectively. Considering that the electronegativity of Cr, Co, Ni, Fe, and Mn atoms are 1.66, 1.88, 1.91, 1.83, and 1.55, respectively,[34] the signs of the calculated average charge transfers for each species are qualitatively consistent with the relative electronegativity (tendency of an atom to attract electrons) between the central atom and the surrounding atoms, i.e., the central atoms with high electronegativity are prone to exhibit negative charge transfer, corresponding to the gain of electrons. For each species in the CrMnFeCoNi, CrFeCoNi, and CrCoNi liquids, there are noticeable fluctuations in the Bader charge, which are expected due to the heterogeneous nature of the local chemical and structural order (i.e., variations in the local composition and bond lengths) around each atom.[35]

To compare the charge transfer between the melts of the CrCoNi-based alloys and typical metallic glasses, Fig. 3(d) shows comparisons of the average absolute value and mean square of the Bader charge transfers for the HEAs considered in the present study with the results for ten typical MGs reported in Ref. 36. Those MG systems were investigated by AIMD, including $Mg_{65}Cu_{25}Y_{10}$, $Ca_{50}Mg_{20}Cu_{30}$, $Ca_{65}Mg_{15}Zn_{20}$, $Ce_{70}Cu_{20}Al_{10}$, $Fe_{80}P_{13}C_7$, $La_{55}Al_{25}Co_{20}$, $Ni_{50}Nb_{50}$, $Zr_{47}Cu_{46}Ag_7$, $Zr_{50}Cu_{50}$, and $Zr_{46}Cu_{46}Al_8$. As shown in Fig. 3(d), the data for the CrMnFeCoNi, CrFeCoNi, and CrCoNi liquids are all located at the bottom left, which represents a low degree of iconicity. At the same time, the charge transfer data for the MGs cover a wide range of values between 0 to 1.1 electrons/atom: the maximum charge transfer values are for $Mg_{65}Cu_{25}Y_{10}$, $Ca_{50}Mg_{20}Cu_{30}$, and $Ca_{65}Mg_{15}Zn_{20}$ liquids, which are all alkaline earth metal based, while only $Fe_{80}P_{13}C_7$ exhibits charger transfer as low as that of CrCoNi-based melts [see Fig. 3(d)]. Such differences in ionicity among the liquids of the CrCoNi-based alloys and the MGs can be understood to originate from the chemistry of the constituents, i.e., the electronegativity difference between the center atom and the surrounding atoms, while their atomic packing structures share similar features of icosahedral short-range order, as will be described further below.

To investigate the atomic structure of the CrCoNi-based melts, we implemented the analysis of pair distribution function (PDF) and structural short-range order, the results of which are shown in Figs. 4 and 5, respectively. Figures

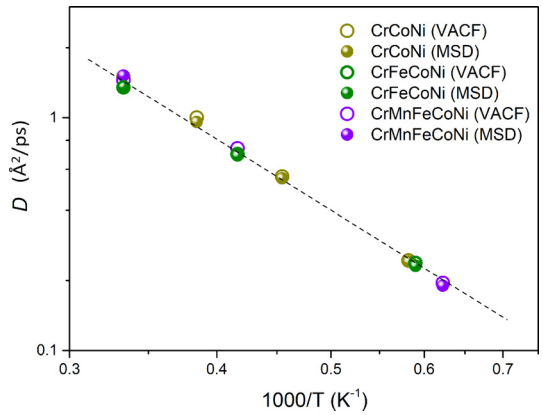

FIG. 2. The concentration-weighted average of the self-diffusion coefficient D for the melts of the CrCoNi, CrFeCoNi, and CrMnFeCoNi alloys computed at different temperatures T. Values of D are calculated from both the MSD and VACF [Eqs. (3) and (4)].

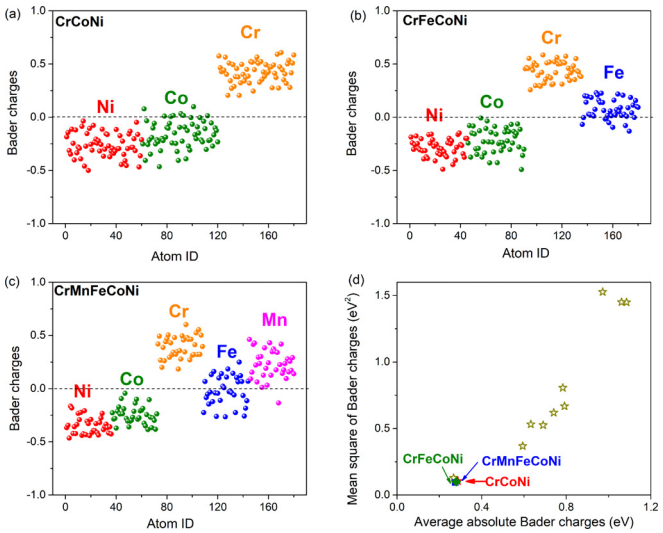

FIG. 3. Charge transfer analysis of the melts of CrCoNi at 1718 K, CrFeCoNi at 1695 K, and CrMnFeCoNi at 1607 K. (a)–(c) The Bader charges for each atom in the three alloy melts, respectively. (d) The average absolute value and mean square of the Bader charge in the melts of the CrCoNi-based alloys as well as the ten typical metallic glasses (MGs) reported in Ref. 36.

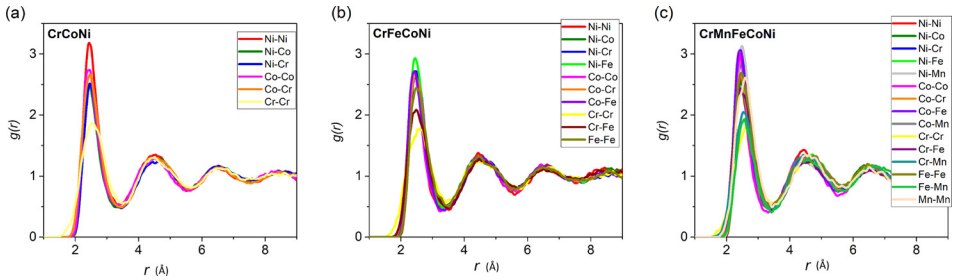

FIG. 4. (a)–(c) The partial PDFs for the melts of the CrCoNi, CrFeCoNi, and CrMnFeCoNi alloys, respectively, at different temperatures.

4(a)–4(c) plot the partial PDFs for the three HEA melts, which exhibit contrasting features as compared to PDFs for the liquids of MGs. Specifically,

(i) The first peak positions for all the partial pairs, such as Cr-Cr, Cr-Ni, Cr-Co, Ni-Ni, etc., are close, which is consistent with the similar atomic size for those elements (i.e., metallic radii for these atoms are: $r_{Cr} = 1.30$ Å, $r_{Co} = 1.28$ Å, $r_{Ni} = 1.28$ Å, $r_{Mn} = 1.32$ Å, and $r_{Fe} = 1.28$ Å);[37]

(ii) The intensities of the first peaks vary, especially for Cr-Cr pairs, which show the lowest intensity but broadest spectrum, as compared to all other pairs (this implies that the partial coordination number of Cr around Cr is close to other pairs). Further analyses indicate no obvious chemical short-range order in those melts, which is in contrast to the observed local chemical ordering in CoCoNi medium-entropy alloy solid solutions.[38–40] Such a difference is expected to originate from the significant entropy contribution in high-temperature liquids, which is expected to disfavor local chemical ordering.

(iii) Beyond the first peak, the partial PDFs of all the pairs nearly overlap. In contrast, the MG systems usually exhibit the well-separated partial PDFs, such as MD-simulated $Cu_{46}Zr_{54}$ in Ref. 41, and AIMD-simulated $Mg_{65}Cu_{25}Y_{10}$ in Ref. 42, which originate from the substantial atomic size difference in MG alloys, as compared to the similarity of atomic size in the CrCoNi-based liquids considered in this study.

Detailed information on the structural short-range order in the melts of CrCoNi-based alloys were analyzed using common-neighbor analysis [Figs. 5(a)–5(c)], which is characterized by a three-number index, *ijk* (for example, 555, 444, 533, etc.).[42,43] Using common-neighbor analysis, different local atomic arrangements can be characterized, such as icosahedral order, crystal-like order, and so forth.[42,43] A significant number of five-fold bonds can be found, indicated by their 555 indices (plus distorted variations with indices of 544 and 433); the fraction was found to be as high as ~70% of the total number of pairs. Interestingly, there is also a quite large number of pairs with indices that are found in crystal-like environments. For example, 10% of the pairs have the 422 indices and 6% of the pairs are of the 421 type. The 422 and 421 indices are typical for bonded pairs in a *hcp*- and *fcc*-like structures, respectively. Such crystal-like short-range order in the melts of HEAs is consistent with that reported for metallic glasses.[42,43] Considering the results of short-range order in Figs. 5(a)–5(c), we can conclude that significant icosahedral order exists in the melts of CrCoNi-based medium- and high-entropy alloys, akin to the icosahedral order that has been observed in a wide range of metallic liquids, including those liquids for MG systems, and elemental crystals.[41]

Finally, we have noted a variety of differences between the liquids of HEAs and MGs, which also correspond to dissimilar behavior in solidificaiton. HEAs and MGs are both formed by mixing multiple metallic elements, but the critical idea underlying the selection of metallic atoms for these two classes of alloys is not the same; the constituents/compositions for HEAs need to favor the formation of single-phase crystalline solid solutions, while the MG systems are prone to destabilize the formation of corresponding crystalline counterparts. For example, the empirical rules for the formation of bulk MGs proposed by Inoue[21] are as follows: alloys should be multicomponent systems consisting of more than three elements, there should be a significant difference in the atomic size ratios (>12%) among the three main constituent elements, and the three main constituent elements should have negative heats of mixing. In contrast, the empirical approach for identifying HEA candidates relies on the small atomic size mismatch and low heats of mixing (both positive and negative),[4,44] which promotes the formation of homogeneous solid solutions by avoiding strong chemical segregation and the formation of stable intermetallics.

In summary, AIMD simulations have been used to characterize several properties of three CrCoNi-based melts corresponding to well-studied medium- and high-entropy alloys: (i) The liquid dynamics, i.e., the diffusion coefficient and corresponding activation energy, are very similar, across

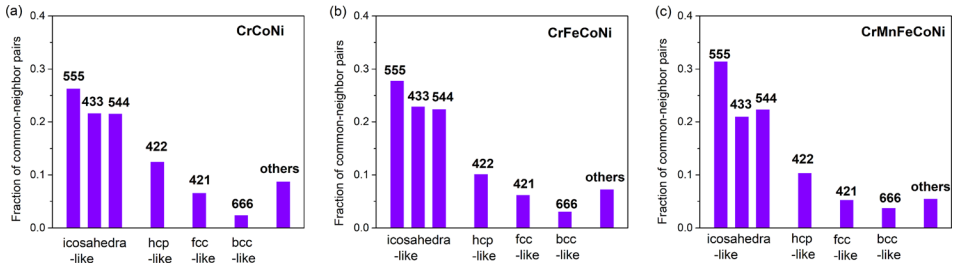

FIG. 5. Short-range order analysis of the melts of CrCoNi (at 1718 K), CrFeCoNi (at 1695 K), and CrMnFeCoNi alloys (at 1607 K). (a)–(c) Their common-neighbor analysis with the fraction of typical common-neighbor pairs, respectively.

the different levels of Fe and Mn concentrations, at the liquidus temperatures and above. (ii) The charge transfer is also significantly smaller in these systems, as compared to those derived in previous studies for the liquids of typical metallic glass systems. Such observations correspond to the similar electronegativity across the constituent species in CrCoNi-based systems. (iii) Similar to the liquids of metallic glass systems, a dominant fraction of icosahedral short-range order is also found among the melts of CrCoNi-based medium- and high-entropy alloy systems, accompanied by a small fraction of crystal-like short-range order. The present results for the melt properties of CrCoNi-based HEAs, and their similarities and differences related to the corresponding properties of the liquid phase of MGs, provides insights into the factors favoring solidification to single-phase solid solutions in HEAs, rather than the stabilization of the amorphous state under moderate cooling rates in MGs.

This work was supported by the Mechanical Behavior of Materials Program (KC13) at the Lawrence Berkeley National Laboratory, funded by the U.S. Department of Energy, Office of Science, Office of Basic Energy Sciences, Materials Sciences and Engineering Division, under Contract No. DE-AC02-05CH11231. The study made use of the resources of the National Energy Research Scientific Computing Center, which is also supported by the Office of Basic Energy Sciences of the U.S. Department of Energy under Contract No. DE-AC02-05CH11231.

[1]J. W. Yeh, S. K. Chen, S. J. Lin, J. Y. Gan, T. S. Chin, T. T. Shun, C. H. Tsau, and S. Y. Chang, Adv. Eng. Mater. **6**, 299–303 (2004).
[2]B. Cantor, I. T. H. Chang, P. Knight, and A. J. B. Vincent, AJB Mater. Sci. Eng. A **375**, 213–218 (2004).
[3]Y. Zhang, T. T. Zuo, Z. Tang, M. C. Gao, K. A. Dahmen, P. K. Liaw, and Z. P. Lu, Prog. Mater. Sci. **6**, 1–93 (2014).
[4]D. B. Miracle and O. N. Senkov, Acta Mater. **122**, 448–511 (2017).
[5]M. C. Troparevsky, J. R. Morris, P. R. C. Kent, A. R. Lupini, and G. M. Stocks, Phys. Rev. X **5**, 011041 (2015).
[6]B. Gludovatz, A. Hohenwarter, D. Catoon, E. H. Chang, E. P. George, and R. O. Ritchie, Science **345**, 1153–1158 (2014).
[7]B. Gludovatz, A. Hohenwarter, K. V. S. Thurston, H. B. Bei, Z. G. Wu, E. P. George, and R. O. Ritchie, Nat. Commun. **7**, 10602 (2016).
[8]Y. W. Zhang, G. M. Stocks, K. Jin, C. Lu, H. Bei, B. C. Sales, L. M. Wang, L. K. Beland, R. E. Stoller, G. D. Samolyuk *et al.*, Nat. Commun. **6**, 8736 (2015).
[9]F. Granberg, K. Nordlund, M. W. Ullah, K. Jin, C. Lu, H. Bei, L. M. Wang, F. Djurabekova, W. J. Weber, and Y. Zhang, Phys. Rev. Lett. **116**, 135504 (2016).
[10]C. Lu, L. Niu, N. Chen, K. Jin, T. Xiu, Y. Zhang, F. Gao, H. Bei, S. Shi, M. R. He *et al.*, Nat. Commun. **7**, 13564 (2016).
[11]G. Laplanche, A. Kostka, O. M. Horst, G. Eggeler, and E. P. George, Acta Mater. **118**, 152–163 (2016).
[12]G. Laplanche, A. Kostka, C. Reinhart, J. Hunfeld, E. Eggeler, and E. P. George, Acta Mater. **128**, 292–303 (2017).
[13]J. Miao, C. E. Slone, T. M. Smith, C. Niu, H. Bei, M. Ghazisaeidi, G. M. Pharr, and M. J. Mills, Acta Mater. **132**, 35–48 (2017).
[14]T. M. Smith, M. S. Hooshmand, B. D. Esser, F. Otto, D. W. McComb, E. P. George, M. Ghazisaeidi, and M. J. Mills, Acta Mater. **110**, 352–363 (2016).
[15]Z. J. Zhang, M. M. Mao, J. Wang, B. Guldovatz, Z. Zhang, S. X. Mao, E. P. George, Q. Yu, and R. O. Ritchie, Nat. Commun. **6**, 10143 (2015).
[16]Z. J. Zhang, H. W. Sheng, Z. J. Wang, B. Gludovatz, Z. Zhang, E. P. George, Q. Yu, and R. O. Ritchie, Nat. Commun. **8**, 14390 (2017).
[17]C. Niu, C. R. LaRosa, J. Miao, M. J. Mills, and M. Ghazisaeidi, Nat. Commun. **9**, 1363 (2018).
[18]S. J. Zhao, G. M. Stocks, and Y. W. Zhang, Acta Mater. **134**, 334–345 (2017).
[19]M. C. Gao and D. E. Alman, Entropy **15**, 4504 (2013).
[20]A. L. Greer, "Metallic glasses," in *Physical Metallurgy*, 5th ed., edited by D. E. Laughlin and K. Hono (Elsevier, 2014), pp. 305–385.
[21]A. Inoue, Acta Mater. **48**, 279 (2000).
[22]G. Kresse and J. Hafner, Phys. Rev. B **47**(1), 558 (1993).
[23]G. Kresse and J. Hafner, Phys. Rev. B **49**, 14251 (1994).
[24]G. Kresse and D. Joubert, Phys. Rev. B **59**, 1758 (1999).
[25]P. E. Blochl, Phys. Rev. B **50**, 17953 (1994).
[26]J. P. J. Perdew, K. Burke, and M. Ernzerhof, Phys. Rev. Lett. **77**, 3865 (1996).
[27]H. Monkhorst and J. Pack, Phys. Rev. B **13**, 5188–5192 (1976).
[28]K. Y. Tsai, M.-H. Tsai, and J.-W. Yeh, Acta Mater. **61**, 4887–4897 (2013).
[29]O. N. Senkov, J. D. Miller, D. B. Miracle, and C. Woodward, Nat. Commun. **6**, 6529 (2015).
[30]M. P. Allen and D. J. Tidesley, *Computer Simulation of Liquids* (Clarendon Press, Oxford, 1989).
[31]C. Woodward, M. Asta, D. R. Trinkle, J. Lill, and S. Angioletti-Uberti, J. Appl. Phys. **107**, 113522 (2010).
[32]R. Bader, *Atoms in Molecules: A Quantum Theory* (Oxford University Press, New York, 1990).
[33]G. Henkelman, A. Arnaldsson, and H. Jónsson, Comput. Mater. Sci. **36**, 354 (2006).
[34]A. L. Allred, J. Inorg. Nucl. Chem. **17**, 215 (1961).
[35]R. F. W. Bader, W. H. Henneker, and P. E. Cade, J. Chem. Phys. **46**, 3341 (1967).
[36]J. Ding and Y. Q. Cheng, Appl. Phys. Lett. **104**, 051903 (2014).
[37]D. B. Miracle, Acta Mater. **54**, 4317–4336 (2006).
[38]J. Ding, Q. Yu, M. Asta, and R. O. Ritchie, PNAS **115**(36), 8919–8924 (2018).
[39]F. X. Zhang, S. J. Zhao, K. Jin, H. Xue, G. Velisa, H. Bei, R. Huang, J. Y. P. Ko, D. C. Pagan, J. C. Neuefeind *et al.*, Phys. Rev. Lett. **118**, 205501 (2017).
[40]A. Tamm, A. Aabloo, M. Klintenberg, M. Stocks, and A. Caro, Acta Mater. **99**, 307–312 (2015).
[41]J. Ding, M. Asta, and R. O. Ritchie, Proc. Natl. Acad. Sci. **114**, 8458–8463 (2017).
[42]J. Ding, Y. Q. Cheng, and E. Ma, Acta Mater. **61**, 3130 (2013).
[43]J. Ding and E. Ma, npj Comput. Mater. **3**, 9 (2017).
[44]S. Guo, Q. Hu, C. Ng, and C. T. Liu, Intermetallics **41**, 96–103 (2013).